Proceedings of the joint ICVRAM ISUMA UNCERTAINTIES conference
Florianópolis, SC, Brazil, April 8-11, 2018

# On the differences in the dynamic response of up-wind and waked wind turbines: Analysis via surrogate Gaussian Process time-series models

**Luis David Avendaño Valencia**[1], **Imad Abdalah**[1], **Eleni N. Chatzi**[1]

[1] Institute of Structural Engineering, ETH Zürich, Stefano-Franscini-Platz 5, 8093 Zürich, Switzerland
avendano@ibk.baug.ethz.ch, abdallah@ibk.baug.ethz.ch

**Keywords.** Wind Turbine, Fatigue, Wake, Dynamic Response, Gaussian Process Surrogate Models

**Abstract.** Wind turbines structures are described by complex dynamics operating under a wide range of environmental and operational conditions. Amongst these, the varying nature of the wind excitation forms perhaps the main driver for the variability of the induced dynamics. In this sense, the features of the dynamic response of an up-wind wind turbine are expected to be differentiated with respect to that of a similar wind turbine receiving the slower, meandering and more turbulent wind stream of a wake. In this context, the main aim of this work is to determine the degree to which the dynamics of up-wind and wake-affected wind turbines results significantly differentiated. To this end, Monte Carlo simulations of the dynamic response of a pair of wind turbines, one in the up-wind position and the other receiving the wake of the first, for several separation distances and under a wide range of atmospheric and inflow conditions are performed. These simulations are subsequently used to identify surrogate global models of the dynamic response of each wind turbine using a Gaussian Process time-series modelling approach. Statistical distance measures are then utilized to determine if the resulting surrogate models are statistically different. In addition, the obtained surrogates are used to determine the long-term loads on the wind turbine, and thus evaluate the accumulated fatigue of the up-wind and wake-affected wind turbines. The results of this study may be used to create more robust damage diagnosis algorithms for wind turbines at the farm level, considering exposure of a wind turbine component in terms of wake. The conclusions drawn will further facilitate the evaluation of fatigue accumulation for wake-affected wind turbines, which is key to the design of the layout of wind farms.

## 1 INTRODUCTION

An important objective of structural health monitoring (SHM) is the life-cycle assessment and the calculation of the remaining useful life-time of structural components, which in turn requires an accurate estimate of the loading pattern on those components. Ideally one would assess fatigue loads on all wind turbines components' in the farm (cluster) by direct and comprehensive measurements. When direct measurements through sensors (e.g. strain gauges, accelerometers) on all turbines are not possible, financially nor operationally feasible or too expensive to implement, one can rely on forward physics-based numerical simulations (of various fidelities), surrogate modelling techniques such as Kriging, Polynomial Chaos Expension, B-splines, ARMA, TV-ARMA, Kalman Filtering, and so on, inverse prediction techniques or a combination thereof. This, though, requires a thorough understanding of the wake effects on non-measured wind turbines in the wind turbines cluster (assuming the availability of loads data from $n$ out of $N$ turbines in the farm ($n \ll N$)). For each of the aforementioned approaches a set of input parameters needs to be specified, measured and/or calibrated with an associated degree of uncertainty. In a setting such as a large wind farm, wakes are known to have significant impact on extreme and fatigue loads. To this end, in this paper we will attempt to analyse the effect of input environmental parameters on the loads patterns of a wind turbine in the wake. More specifically, in the context of SHM it is important to define what features to look for (what to measure) and how accurately to measure these features. The subsequent analysis will be put in this context rather than focusing on the Aerodynamics/Fluid dynamics aspects of this problem.

Wind turbines significantly disturb the properties of a wind flow passing through the rotor as the kinetic energy of the wind is converted to mechanical energy. The region of air affected by the rotor is termed the wind turbine *wake*. The wind turbine wake is characterized by increased fluctuations in the wind speed (turbulence) and lowered average wind speed (wake deficit). Consequently, both the power performance and the dynamic response of an up-wind wind turbine are expected to differ from that of a similar wind turbine receiving the wake of the first one (Lee et al., 2012).

In general, it is accepted that loads in some wind turbine components are driven by random large scale wake movements, known as wake meandering. At the same time, loads in other components are influenced by small-scale turbulence due the breakdown of tip vortices and turbulence generated by the shear layer in the edges of the wake. Thus, it is simply not sufficient to describe the wake in terms of long term averages of wind speed and turbulence intensity, as this does not accurately capture the overall wake effects on wind turbine loads (Keck, 2013). An extensive body of literature has

investigated the effects of wind turbine wakes on extreme and fatigue loads, including Vølund, (1992), Frandsen and Thoegersen, (2000), Frandsen, (2007), Schmidt et al., (2011), Lee et al., (2012), and Larsen et al., (2013). However, studying the effect of wakes in wind turbine clusters has garnered much less attention within the structural health monitoring community, where one is mostly interested in damage diagnosis and assessment of useful remaining lifetime of components using a minimum number of sensors.

In fact, only recently the effects of changing environmental and operational conditions in wind turbine dynamics have been recognized in the operational modal analysis and structural health monitoring community (Ozbek, Meng and Rixen, 2013; Häckell and Rolfes, 2013; Shirzadeh et al., 2013; Avendaño-Valencia and Fassois, 2014; Avendaño-Valencia et al., 2017). A main challenge stems from the modeling of the very complex global dynamics of wind turbines and isolation of sources of variation. Recent contributions of the authors have attempted towards a holistic modeling of the dynamic response of wind turbines by means of *Linear Parameter Varying AutoRegressive* (LPV-AR) models to describe the dynamics on short periods of time in combination with Gaussian Process (GP) regression to describe the variation in the model parameters in accordance to measurable environmental and operational parameters (Avendaño-Valencia et al., 2017; Avendaño-Valencia and Chatzi, 2017). The postulated GP-LPV-AR models offer provide an efficient means to represent the non-stationary dynamic response of a structure under changing environmental and operational conditions.

The main aim of this work is to study the effects of wakes on wind turbine loads under variable environmental and operational conditions. To this end we consider two approaches: (1) short-term *Damage Equivalent Load* (DEL) analysis, and (2) analysis of the wind turbine loads by means of Gaussian Process time-series modeling. A full factorial design of experiments is appraised to examine the effects on the simulated structural dynamics due to variations in various operational variables, including mean wind speed, inflow turbulence intensity, wind shear and the spacing between turbines (measured in multiples of rotor diameters). All simulations are performed using the *Dynamic Wake Meander* (DWM) model (Madsen et al., 2003) coupled into the FAST wind turbine aeroelastic and system dynamics simulator (Jonkman and Buhl, 2005). This coupling is well documented in the work by Hao et al. (2014).

In the short-term DEL analysis, we consider the uncertainty in the material properties by varying the Wöhler exponent in the damage equivalent load calculations. Initially, a broad DEL analysis is performed on the whole set of simulations, while detailed analyzes are presented based on a more granular combinations of operational conditions. Subsequently, the simulated loads of the up-wind and waked wind turbines are further analyzed in terms of baseline GP-LPV-VAR model, which is used as a surrogate for the wind turbine load dynamics in the tower base and blade root as a function of the mean wind speed and turbulence intensity. Such baseline model is constructed from a second set of FAST-based simulations on a dense grid of wind speeds and turbulence intensities.

The remainder of this article is organized as follows. In section 2, we elaborate on the dynamic wake and aeroelastic wind turbine simulations setup and we provide a short reminder of how the short-term fatigue damage equivalent loads are calculated. In section 3, we revisit the theory of Gaussian process time series modelling to identify surrogate global models of the dynamic response of wind turbines. In section 4, we present the main results where we compare the fatigue loads pattern of the up-wind and wake-affected wind turbines, and similarly compare the dynamics of the up-wind and wake-affected wind turbines through the Gaussian process time series analysis.

## 2 DYNAMIC WAKE AND AEROELASTIC SIMULATIONS

In this section, we demonstrate the wind turbine wake and aeroelastic loads simulations, carried out via use of the dynamic wake meander model (DWM; Madsen et al., 2003, Thomsen et al., 2003) coupled into FAST wind turbine aeroelastic simulator (Jonkman and Buhl, 2005). We focus on the flapwise bending moment at the blade root ($M_b$) and tower bottom fore-aft bending moment ($M_t$) as illustrated in Fig. 1.

### 2.1 Dynamic Wake Meandering (DWM) and Stochastic aeroelastic simulations

FAST is a wind-turbine-specific time domain aeroelastic computer simulator that employs a combined modal and multibody dynamics formulation, adopting limited degrees of freedom (DOF). Since FAST models flexible elements using a modal representation, the reliability of this representation depends on the generation of accurate mode shapes by the engineer, which are then used as input into FAST. Large structural elements, such as blades and tower models, are characterized by properties such as stiffness and mass per unit length to represent the flexibility characteristics. FAST models the turbine using 24 DOF, including two blade-flap modes and one blade-edge mode per blade, two fore-aft and two side-to-side tower bending modes, nacelle yaw, the generator azimuth angle and the compliance in the drive train between the generator and hub/rotor. The aerodynamic model is based on the Blade Element Momentum theory (including skew inflow, dynamic stall and generalized dynamic wake). The stochastic input wind field uses the Kaimal turbulence model (Kaimal, Wyngaard and Coté, 1972). Aeroelastic simulations of wind turbines are stochastic largely due to the stochastic nature of the input wind field and to a lesser but not insignificant degree owing to the response of the control system. To illustrate this we plot in Fig. 2(a) two replications with the same rotor averaged wind speed time series with mean value of $U = 7\ m/s$, turbulence intensity of $Ti = 5\ \%$ and wind shear exponent of $\alpha = 0.2$. The corresponding output times series of the blade root flapwise bending moment are plotted in Fig. 2(b ). We observe that given the same rotor averaged wind field characteristics, the response of the blade in replication #1 differs from that in replication #2. Thus,

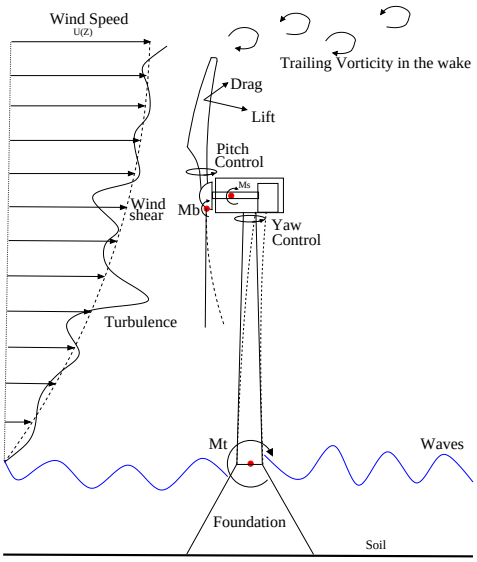


Figure 1: Schematic of a wind turbine: $M_b$ is the flapwise bending moment at the blade root. $M_t$ is the tower bottom fore-aft bending moment. $U(Z)$ is the mean wind speed at height $Z$. Vertical wind shear is depicted by the dotted grey line and turbulence by the thick black line.

it is common practice to generate a significant number of stochastic simulations for various operating and environmental conditions in order to cover variability on aeroelastic fatigue and extreme analysis (more on this in section 2.2).

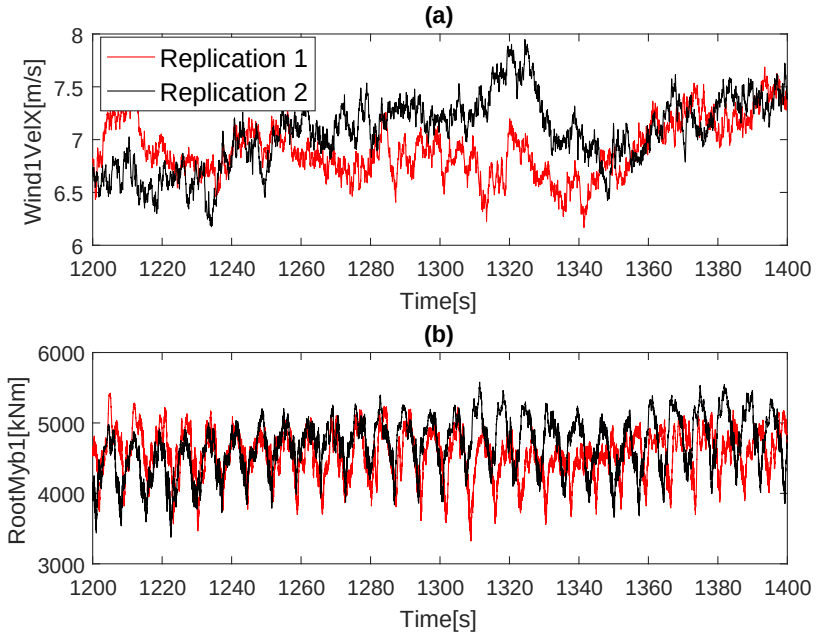


Figure 2: (a) Time series of the rotor averaged wind speed. In both replications the mean wind speed is $U = 7\ m/s$, turbulence intensity is $Ti = 5\ \%$ and wind shear exponent is $\alpha = 0.2$. (b) Time series of the blade root flapwise bending moment. The response differs in replication #1 versus replication #2.

Wind turbines located in wind farms experience a wind field that is modified compared to the undisturbed ambient wind field. A wake is characterized by a decrease in the mean wind speed and increase in wind speed fluctuations (turbulence) behind a turbine. The downstream transport of a wake follows a stochastic pattern known as wake meandering (oscillations). It appears as an intermittent phenomenon, where winds at down-wind positions may be undisturbed for part of the time, but interrupted by episodes of intense turbulence and reduced mean speed as the wake hits the observation point (Larsen et al., 2007). Thus, a correct wind turbine load prediction requires the inclusion of the downstream evolution of wake deficit, the increased small-scale wake turbulence and the wake meandering. In this paper we choose to use the DWM wake model coupled to FAST following the NREL implementation. This coupling is well documented in the work by Hao et al. (2014). The dynamic wake meander model coupled into FAST wind turbine aeroelastic tool is used to model the up-wind (Turbine 1 in Fig. 3) wind turbine's wake effect on the structural dynamics of the down-wind wake-affected

turbine (Turbine 2 in Fig. 3). While FAST is simulating an up-wind turbine, DWM calculates the wake deficit velocity, the meandered wake center positions with respect to time, and the added turbulence intensity due to the presence of the wake mixing. While a down-wind wake-affected turbine is being simulated in FAST, the inflow wind to this wake-affected turbine is modified based on the wake modelling results of its up-wind turbines. Thus the effect of the wakes can be accurately reflected on the wake-affected turbine according to its immediate wake (Hao et al., 2014).

### 2.2 Description of the wind turbines and computational domain

The simulations in DWM-FAST considered two reference NREL three-bladed up-wind, horizontal-axis wind turbines (Jonkman et al., 2009) with 126 $m$ rotor diameter, 5 $MW$ rated power and hub height of 90 $m$. The rated power of 5 $MW$ occurs at a wind speed of 11.4 $m/s$ and a rotor speed of 12.1 $RPM$. We list some of the more important properties of the simulated wind turbine in Tab. 1. In the DWM setup the two turbines are perfectly aligned in such a way that the down-wind wind turbine experiences a single full wake (see Fig. 3). Furthermore, the yaw angle was fixed at zero degrees relative to their neutral frame of reference, and the ambient wind field is also perfectly aligned with the rotor of the up-wind wind turbine, i.e. no yaw misalignment is introduced.

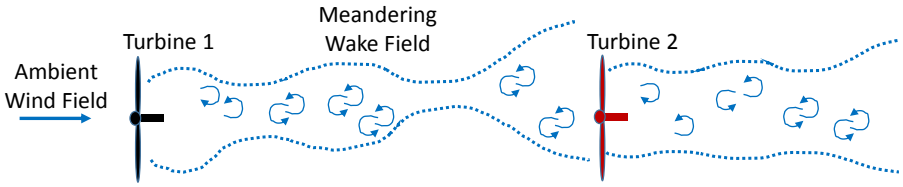


Figure 3: Schematic of an up-wind and down-wind (wake-affected) wind turbine with a single meandering wake field in between.

Table 1: Properties of the NREL 5-MW reference wind turbine.

| | |
|---|---|
| Number of blades | 3 |
| Rotor diameter | 126 $m$ |
| Hub height | 90 $m$ |
| Rated power | 5 $MW$ |
| Cut-in wind speed | 3 $m/s$ |
| Cut-out wind speed | 25 $m/s$ |
| Control | Variable Speed, Collective Pitch |
| Variable speed | from cut-in to cut-out wind speed |
| Variable pitch | from cut-in to cut-out wind speed |
| Rated wind speed | 11.4 $m/s$ |
| Cut-in and rated RPM | $6.9 - 12.1$ $RPM$ |

The variation in the structural dynamics and loads of the up-wind and down-wind wind turbines are significantly dependent on the turbulence inherent in the wind field (ambient free-stream and wake) as well as factors such as the wind shear, the mean wind speed and the spacing between the rotors of turbines 1 and 2 (Fig. 3). Turbulence intensity is given by $Ti = \sigma_U/U$ where $\sigma_U$ is the standard deviation (or turbulence) and $U$ is the mean of the wind speed time series. The wind profile above ground level is expressed using the power law relationship, which defines the mean wind speed $U$ at a height $Z$ above ground using the wind speed $U_{hub}$ measured at hub height $Z_h$ as reference:

$$\frac{U}{U_{hub}} = \left(\frac{Z}{Z_h}\right)^{\alpha} \tag{1}$$

where $\alpha$ is a constant called the *shear exponent*. A full factorial design of experiments is proposed in Tab. 2 to examine the effects on the simulated structural dynamics due to variations in wind speed, inflow turbulence intensity, shear and the turbines' spacing. For each combination of mean wind speed $U$, turbulence intensity $Ti$, shear exponent $\alpha$ and spacing (multiple of rotor diameters D), we generate 12 realizations of the ambient wind field, run DWM-FAST for both turbines and thus resulting in a total of $1,296$ simulated time series. The total length of each time series is 1800 s, for each turbine at the two locations, with a time step of 0.005 s (200 Hz). Note that for each simulation, a total of 2000 s of data is recorded of which the initial 200 s transient data are disregarded. The retained output response in the subsequent analysis are the blade root flapwise bending moment and tower bottom fore-aft bending moment.

Table 2: Design of experiments for the DWM-FAST simulations.

| Mean wind speed $U$ [m/s] | Turb. intensity $Ti$ [m/s] | Shear exponent $\alpha$ [-] | Spacing |
|---|---|---|---|
| $7, 11.5, 20$ | $5, 10, 20$ | $0, 0.2, 0.5$ | $3D, 8D$ |

### 2.3 Fatigue

In addition to the Gaussian process time-series analysis described in the next section, we compare the the short-term fatigue damage equivalent loads (DEL) of the up-wind and down-wind wake-affected wind turbines. The DEL is calculated on the basis of the output loads times series:

$$DEL = \left( \frac{1}{N_{eq}} \sum_i n_i D_i^m \right)^{1/m} \tag{2}$$

where for one output time series, $n_i$ is the number of load cycles with range $D_i$ in the $i$-th range bin of the fatigue load spectrum, $m$ is the Whöler exponent of the relevant material (inverse of S-N curve slope), and $N_{eq}$ is the equivalent number of load cycles, typically $10^7$ cycles. Furthermore, we consider the material properties uncertainties by varying the Wöhler exponent in the damage equivalent loads calculations as shown in Tab. 3.

Table 3: Variations in Wöhler exponent for steel (tower) and composites (blade).

| Tower (steel) | Blade (Composites) |
|---|---|
| $3, 4$ | $10, 11, 12$ |

## 3 GAUSSIAN PROCESS TIME-SERIES MODELLING

### 3.1 Main definitions

Consider the $n$-dimensional response vector $\boldsymbol{y}[t] \in \mathbb{R}^n$ of an system with slowly varying dynamics, which are determined by different *Environmental and Operational Parameters* (EOPs) (wind, temperature, and so on) on a specific time period of length $T$. Among these, a subset of measurable EOPs is denoted by the EOP vector $\boldsymbol{\xi} \in \mathbb{R}^m$. A Gaussian Process (GP) time-series model of the response vector is defined by means of the following equations (Avendaño-Valencia et al., 2017):

$$\boldsymbol{y}[t] = \boldsymbol{\phi}^T[t] \cdot \boldsymbol{\theta} + \boldsymbol{w}[t], \qquad \boldsymbol{w}[t] \sim \texttt{NID}\left(\boldsymbol{0}_{n\times 1}, \boldsymbol{\Sigma}_w\right) \tag{3a}$$

$$\boldsymbol{\theta} = \boldsymbol{M} \cdot \boldsymbol{g}(\boldsymbol{\xi}) + \boldsymbol{u}, \qquad \boldsymbol{u} \sim \mathcal{N}\left(\boldsymbol{0}_{d\times 1}, \boldsymbol{\Sigma}_\theta\right) \tag{3b}$$

where $\boldsymbol{\phi}[t] \in \mathbb{R}^{d\times n}$ is the regression matrix, $\boldsymbol{\theta} \in \mathbb{R}^d$ is a random parameter vector, and $\boldsymbol{w}[t] \in \mathbb{R}^n$ is a vector *Normally and Identically Distributed* (NID) innovations, with zero mean and covariance matrix $\boldsymbol{\Sigma}_w$. The random parameter vector is Gaussian distributed and determined by the coefficient matrix $\boldsymbol{M} \in \mathbb{R}^{d\times p}$, the GP functional basis $\boldsymbol{g}(\boldsymbol{\xi}) \in \mathbb{R}^p$, and the parameter covariance matrix $\boldsymbol{\Sigma}_\theta$.

The GP time-series model is characterized by the following conditional Gaussian distributions (Avendaño-Valencia et al., 2017):

$$p(\boldsymbol{y}[t]|\boldsymbol{\theta}, \mathcal{P}) = \mathcal{N}\left(\boldsymbol{\phi}^T[t] \cdot \boldsymbol{\theta}, \boldsymbol{\Sigma}_w\right) \tag{4a}$$

$$p(\boldsymbol{\theta}|\boldsymbol{\xi}, \mathcal{P}) = \mathcal{N}(\boldsymbol{M} \cdot \boldsymbol{g}(\boldsymbol{\xi}), \boldsymbol{\Sigma}_\theta) \tag{4b}$$

where $\mathcal{P} \triangleq \{\boldsymbol{M}, \boldsymbol{\Sigma}_w, \boldsymbol{\Sigma}_\theta\}$ denotes the set of *hyperparameters* of the model, $p(a|b)$ denotes the conditional distribution of the random variable $a$ given event $b$, and $\mathcal{N}(\boldsymbol{\mu}, \boldsymbol{S})$ indicates a multivariate Gaussian distribution with mean $\boldsymbol{\mu}$ and covariance matrix $\boldsymbol{S}$.

Any type of inferences regarding to the response vector, model parameters and hyperparameters can be performed with the help of Eq. (4). Model identification, requiring the estimation of the hyperparameters and selection of the model structure follows from different estimation schemes hinged on Eq. (4), as explained in (Avendaño-Valencia et al., 2017). In turn, when a GP time-series model is available, then it is possible to evaluate if a test vibration response $\boldsymbol{y}_u[t]$, $t = 1, \ldots, N$ acquired under operational conditions $\boldsymbol{\xi}_u$, corresponds to the identified GP time-series model by evaluating the marginal likelihood (Avendaño-Valencia et al., 2017):

$$p(\boldsymbol{y}_u[t]|\boldsymbol{\xi}_u, \mathcal{P}) = \int_\Theta p(\boldsymbol{y}_u[t]|\boldsymbol{\theta}, \mathcal{P}) \cdot p(\boldsymbol{\theta}|\boldsymbol{\xi}_u, \mathcal{P})\, \mathrm{d}\boldsymbol{\theta} = \mathcal{N}\left(\hat{\boldsymbol{y}}_{\mathrm{pr}}[t|t-1], \boldsymbol{\Sigma}_\varepsilon[t]\right) \tag{5}$$

where $\Theta$ is the domain of integration of the marginalizing integral, $\hat{\boldsymbol{y}}_{\mathrm{pr}}[t|t-1] = \boldsymbol{\phi}_u^T[t] \cdot (\boldsymbol{M} \cdot \boldsymbol{g}(\boldsymbol{\xi}_u))$ is the *a priori* one-step-ahead model predictions and $\boldsymbol{\Sigma}_\varepsilon[t] = \boldsymbol{\Sigma}_w + \boldsymbol{\phi}_u^T[t] \cdot \boldsymbol{\Sigma}_\theta \cdot \boldsymbol{\phi}_u[t]$ is the prediction error covariance matrix. In a similar

form, it is possible to determine if some parameter estimates $\boldsymbol{\theta}_u$ extracted from the test vibration response correspond to the identified GP time-series model by evaluating the probability $p(\boldsymbol{\theta}_u|\boldsymbol{\xi}_u, \mathcal{P})$.

Since the involved densities are multivariate Gaussian, then both tests can be summarized into the following Mahalanobis distances:

$$d_\theta(\boldsymbol{\theta}_u, \boldsymbol{\theta}_o) = (\boldsymbol{\theta}_u - \boldsymbol{\theta}_o)^T \cdot \boldsymbol{\Sigma}_\theta^{-1} \cdot (\boldsymbol{\theta}_u - \boldsymbol{\theta}_o) \tag{6a}$$

$$d_y(\boldsymbol{y}_u, \hat{\boldsymbol{y}}_{pr}) = \frac{1}{N}\sum_{t=1}^{N} (\boldsymbol{y}_u[t] - \hat{\boldsymbol{y}}_{pr}[t|t-1])^T \cdot \boldsymbol{\Sigma}_\varepsilon^{-1}[t] \cdot (\boldsymbol{y}_u[t] - \hat{\boldsymbol{y}}_{pr}[t|t-1]) \tag{6b}$$

where $\boldsymbol{\theta}_o = \boldsymbol{M} \cdot \boldsymbol{g}(\boldsymbol{\xi}_u)$ is the mean parameter vector predicted the the GP time-series model.

### 3.2 GP-LPV-VAR models

The specific type of GP time-series model is determined by the structure of the regression matrix. In the present context, considering the vibration response of a wind turbine, the selected time-series model corresponds to a *Linear-Parameter-Varying Vector AR* (LPV-VAR) model, which is defined as (Avendaño-Valencia, Chatzi, and Fassois, 2017):

$$\boldsymbol{y}[t] = \sum_{i=1}^{n_a} \boldsymbol{A}_i(\beta[t]) \cdot \boldsymbol{y}[t-i] + \boldsymbol{w}[t], \qquad \boldsymbol{w}[t] \sim \texttt{NID}\,(\boldsymbol{0}_{n\times 1}, \boldsymbol{\Sigma}_w) \tag{7a}$$

$$\boldsymbol{A}_i(\beta[t]) = \sum_{j=1}^{p_f} \boldsymbol{A}_{i,j} \cdot f_j(\beta[t]) \cdot \boldsymbol{y}[t-i] \tag{7b}$$

where $\boldsymbol{A}_i(\beta[t]) \in \mathbb{R}^{n\times n}$ is the $i$-th LPV parameter matrix depending on the instantaneous rotor angle $\beta[t]$, and $n_a$ is the autoregressive order. The LPV parameter matrices are projected into a functional basis, where $\boldsymbol{A}_{i,j} \in \mathbb{R}^{n\times n}$ are the matrices with the coefficients of projection, $p_f$ is the order of LPV functional basis, and $f_j(\beta[t])$, $j = 1, \ldots, p_f$ is the $j$-th LPV functional basis. After combining both equations in Eq. (7) and fixing the terms into matrices, leads to the following regression form of the LPV-VAR model (Avendaño-Valencia, Chatzi, and Fassois, 2017):

$$\boldsymbol{y}[t] = \boldsymbol{\phi}^T[t] \cdot \boldsymbol{\theta} + \boldsymbol{w}[t], \qquad \boldsymbol{\phi}[t] = \boldsymbol{I}_n \otimes \boldsymbol{z}[t], \qquad \boldsymbol{\theta} = \mathrm{vec}(\boldsymbol{A}) \tag{8}$$

where $\boldsymbol{I}_n$ indicates the $n$-dimensional identity matrix, $\otimes$ indicates the Kronecker product, and $\mathrm{vec}(\boldsymbol{A})$ is the vectorization operator, which stacks the columns of a matrix into a single column vector. In addition, the matrix $\boldsymbol{A}$ and the vector $\boldsymbol{z}[t]$ are defined as follows:

$$\boldsymbol{A} = \left[\boldsymbol{A}_{1,1} \cdots \boldsymbol{A}_{1,p_f} \,|\, \boldsymbol{A}_{2,1} \cdots \boldsymbol{A}_{2,p_f} \,|\, \cdots \,|\, \boldsymbol{A}_{n_a,1} \cdots \boldsymbol{A}_{n_a,p_f}\right]^T_{n\cdot n_a \cdot p_f \times n}, \qquad \boldsymbol{z}[t] = \begin{bmatrix} \boldsymbol{f}(\beta[t]) \otimes \boldsymbol{y}[t-1] \\ \boldsymbol{f}(\beta[t]) \otimes \boldsymbol{y}[t-2] \\ \vdots \\ \boldsymbol{f}(\beta[t]) \otimes \boldsymbol{y}[t-n_a] \end{bmatrix}_{n\cdot n_a \cdot p_f \times 1}$$

where $\boldsymbol{f}(\beta[t]) = \begin{bmatrix} f_1(\beta[t]) & f_2(\beta[t]) & \cdots & f_{p_f}(\beta[t]) \end{bmatrix}^T$.

### 3.3 Reduced model size by Principal Component Regression

The parametrization of the LPV-VAR model has been used by several authors before, however it is characterized by a very large number of parameters and large-sized matrices. Further expansion of the LPV-VAR model into the GP time-series structure would lead to an even larger number of parameters, which would hinder estimation, and increase the computational and storage requirements. To alleviate this problem, a *Principal Component Regression* (PCR) approach is utilized to reduce the size of the representation. To that end, consider the sample regression matrix $\boldsymbol{\Phi} \in \mathbb{R}^{d\times N_T}$ with $N_T = n \cdot N \cdot N_s$, defined as:

$$\boldsymbol{\Phi} = \left[\boldsymbol{\phi}_1[1] \cdots \boldsymbol{\phi}_1[N] \,|\, \boldsymbol{\phi}_2[1] \cdots \boldsymbol{\phi}_2[N] \,|\, \cdots \,|\, \boldsymbol{\phi}_{N_s}[1] \cdots \boldsymbol{\phi}_{N_s}[N]\right]$$

where $\boldsymbol{\phi}_r[t]$ is the regression matrix corresponding to the $r$-th vibration response sample out of $N_s$ total samples evaluated at time $t$. The *Singular Value Decomposition* (SVD) of the sample regression matrix takes for form:

$$\boldsymbol{\Phi} = \boldsymbol{U} \cdot \boldsymbol{\Lambda} \cdot \boldsymbol{V}^T \tag{9}$$

where $\boldsymbol{U} \in \mathbb{R}^{d\times d}$ and $\boldsymbol{V} \in \mathbb{R}^{N_T \times N_T}$ are the left and right eigenvector matrices, and $\boldsymbol{\Lambda} \in \mathbb{R}^{d\times N_T}$ is the diagonal eigenvalue matrix. The SVD in Eq. (9) can be understood a two different components, the first one is a projection matrix corresponding to the left eigenvector matrix $\boldsymbol{U}$, while the second is a matrix of orthogonal regressors $\boldsymbol{\Phi}_{\text{orth}}$, defined as:

$$\boldsymbol{\Phi}_{\text{orth}} \triangleq \boldsymbol{\Lambda} \cdot \boldsymbol{V}^T = \left[\boldsymbol{\varphi}_1[1] \cdots \boldsymbol{\varphi}_1[N] \,|\, \boldsymbol{\varphi}_2[1] \cdots \boldsymbol{\varphi}_2[N] \,|\, \cdots \,|\, \boldsymbol{\varphi}_{N_s}[1] \cdots \boldsymbol{\varphi}_{N_s}[N]\right] \tag{10}$$

In this form, $\boldsymbol{\phi}_r[t] = \boldsymbol{U} \cdot \boldsymbol{\varphi}_r[t]$. Therefore, the LPV-VAR model in regression form shown in Eq. (8) may be cast into the alternative regression form (Avendaño-Valencia et al., 2017):

$$\boldsymbol{y}[t] = (\boldsymbol{U} \cdot \boldsymbol{\varphi}_r[t])^T \cdot \boldsymbol{\theta} + \boldsymbol{w}[t] = \boldsymbol{\varphi}_r^T[t] \cdot \boldsymbol{\vartheta} + \boldsymbol{w}[t] \tag{11}$$

where $\boldsymbol{\vartheta} = \boldsymbol{U}^T \cdot \boldsymbol{\theta}$ is the transformed parameter vector. Moreover, dimensionality reduction can be achieved by selecting a subset of regressors from $\boldsymbol{\varphi}_r^T[t]$ corresponding to the first $\tilde{d}$ eigenvalues. Thus, regression is based instead on the trimmed projection and regression matrices:

$$\tilde{\boldsymbol{U}} = \begin{bmatrix} \boldsymbol{u}_1 & \boldsymbol{u}_2 & \cdots & \boldsymbol{u}_{\tilde{d}} \end{bmatrix} \in \mathbb{R}^{d \times \tilde{d}}, \qquad \tilde{\boldsymbol{\varphi}}_r[t] = \begin{bmatrix} \varphi_{1,1,r}[t] & \varphi_{1,2,r}[t] & \cdots & \varphi_{1,n,r}[t] \\ \varphi_{2,1,r}[t] & \varphi_{2,2,r}[t] & \cdots & \varphi_{2,n,r}[t] \\ \vdots & \vdots & \ddots & \vdots \\ \varphi_{\tilde{d},1,r}[t] & \varphi_{\tilde{d},2,r}[t] & \cdots & \varphi_{\tilde{d},n,r}[t] \end{bmatrix}_{\tilde{d} \times n} \tag{12}$$

where $\boldsymbol{u}_l$ corresponds to the columns of $\boldsymbol{U}$.

The PCR-based regression has several important advantages: (*i*) The regression is hinged on uncorrelated regressors. In consequence regressors may be discarded without removing information on other regressors. In addition the parameters of the representation are also uncorrelated, which further simplifies the computation of the global GP-LPV-VAR model. (*ii*) There is an important reduction in the number of parameters of the model and the overall model size. (*iii*) The parameters in the original representation, which may be useful for further dynamic analyzes, can be retrieved through the operation $\boldsymbol{\theta} = \boldsymbol{U} \cdot \boldsymbol{\vartheta}$. If dimensionality reduction is not attempted, then the parameter vector in the PCR approach should be equal to that of the original representation with some negligible numerical difference. Otherwise, the error would become a function of the number of reduced dimensions. Therefore, it is essential to determine an optimal value for the dimensionality of the reduced model. This is typically achieved through examination of the curve of normalized cumulative sum of eigenvalues.

## 4 RESULTS AND DISCUSSIONS

In discussing the details of the effect of the environmental variables on the short-term DEL of the tower and blade, it is important to have an understanding of the wind turbine operation in relation to the wake formation and transport. We provide a brief summary on this subject.

A wind turbine operates in mainly three characteristically different regions. At *wind speeds* below rated (corresponding to the rated power of the wind turbine, typically $\sim 9-12\ m/s$) the turbine attempts to run on optimal pitch and tip speed ratio to extract as much power as possible from the wind. This results in a nearly constant induction factor at optimal levels ($\sim 0.3$). At wind speeds above rated, the wind turbine controller aims at maintaining rated power by maintaining a constant rotor speed. This means a less efficient power extraction from the wind by gradually pitching towards smaller angles of attack with increasing mean wind speed in combination with allowing the tip-speed ratio to fall (due constant rotor speed at higher wind speeds). Thus reducing the turbine induction. The distribution of induction over the rotor essentially governs the evolution and transport of the wake (Keck, 2013). As the rotor rotates, vortices are shed from the tip of the blades and are transported down-wind into the wake. With higher tip-speed ratios (low mean wind speeds) the vortices are released at higher rate causing them to interact and break down, which adds to the turbulent mixing and recovery of the wake deficit. Between the two aforementioned regions there exists a smooth transition region (region 2.5). This is a region typically characterized by the initation of deviation from optimal power extraction, but also typically maximum thrust driven loads.

For its part, the ambient *turbulence intensity* is the most important parameter for wake evolution (Keck, 2013). The interaction between the wake boundary and the ambient turbulence dominates the process of the wake deficit diffusion which causes a more uniform and more symmetrical wake flow field. Finally, *wind shear* causes periodically one part of the rotor to have a higher induction, which causes the wake deficit to be less symmetric. Meaning that elevated wind shear reduces the overall efficiency of the rotor though creating a less severe wake in the process.

### 4.1 Short-term damage equivalent load analysis

The probabilities of exceedance for $M_b$ and $M_t$ (Fig. 4) are computed from the raw rainflow cycle counted data for each simulated time series. The up-wind wind turbine exhibits the largest (worst) DEL loads for both blade and tower, which is a surprising result. Fig. 4 considered the calculated DEL for all combination of wind speed $U$, turbulence intensity $Ti$, shear exponent $\alpha$, spacing (multiple of rotor diameters $D$) and Wöhler exponents. This is a blind comparison with no a-priori discrimination on environmental and operating conditions.

Let us drill down on the results and analyse the elementary effects of each of the input random variables, namely the mean wind speed $U$, turbulence intensity $Ti$, shear exponent $\alpha$ and spacing (multiple of rotor diameters D). To further this analysis, and to better understand the effect of wake physics on wind turbine fatigue loads, we supplement the DWM-FAST simulations with FAST aeroelastic simulations of a standalone wind turbine with input turbulent inflow

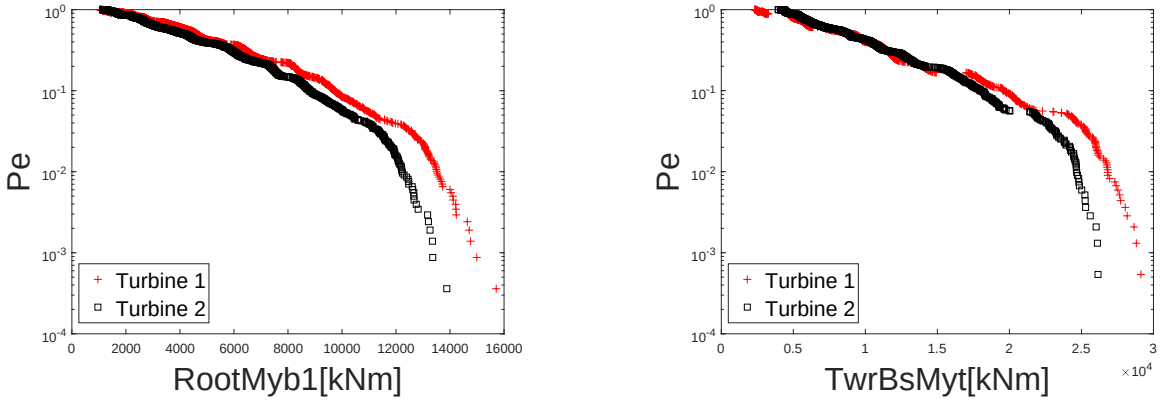


(a) (b)

Figure 4: (a) Probability of exceedance of short-term DEL blade root flapwise bending moment and (b) tower bottom fore-aft bending moment for all simulated data in the design of experiments.

characteristics corresponding to rotor averaged inflow conditions derived by DWM on both up-wind and down-wind wind turbines. We show results for the different Wöhler exponent (tower-steel and blade-composites) to interpret how components with large Wöhler values are sensitive to the few large load cycles, whereas components with small Wöhler values are sensitive to many small cycles.

#### *4.1.1 Tower*

In Fig. 5(a)-7(a) the ambient free-stream mean wind speed is $U = 7\ m/s$, which means that the up-wind wind turbine is operating below rated power corresponding to high thrust coefficient and high induction. The DEL of the down-wind (wake-affected) wind turbine is higher compared to DEL of the up-wind wind turbine. The high thrust and high induction from the up-wind wind turbine lead to a drop in the mean wind speed and an increase in the turbulence intensity of the transported wake towards the down-wind turbine. Both the standalone FAST and DWM-FAST simulations results indicate the same trend for the up-wind wind turbine, not so for the down-wind wake-affected wind turbine. This difference becomes more pronounced (but not significant) for higher ambient turbulence intensities (e.g. $Ti \geq 10\ \%$) which suggests that introducing the correct wake physics into such analysis is crucial. In an SHM context, this points out that, in the absence of direct loads measurements on a wake-affected wind turbine, quantifying the mean wind speed and turbulence intensity for the purpose of surrogating/predicting the structural fatigue loads is necessary but not sufficient, additional signals indicating the wake signature are required. Similar results are generally observed for a separation distance of $D = 8$ rotor diameters between the up-wind and down-wind wind turbines.

In Fig. 5(b)-7(b) the ambient free-stream mean wind speed is $U = 11.5\ m/s$ which means that the up-wind wind turbine is operating around rated wind speed ("knee" of the power curve) corresponding to a lower thrust coefficient and lower induction. Except when the turbulence intensity is low ($Ti = 5\ \%$), the DEL of the down-wind (wake-affected) wind turbine becomes lower compared to DEL of the up-wind wind turbine. Both the standalone FAST and DWM-FAST simulations results indicate the same trend. Two variables are at play here, the mean wind speed drops, while the turbulence intensity increases but not at the same rate observed at lower ambient mean wind speeds. The effects depend strongly on the intensity of the ambient turbulence relative to the velocity deficit in the wake. At elevated mean wind speeds the thrust coefficient and induction drop result in a less efficient transport of the wake. Hence the impact on the DEL of lower mean wind speed in front of the wake-affected wind turbine is more pronounced compared to the increase in turbulence intensity. At such an elevated up-wind mean wind speed and for all turbulence intensity levels, the standalone FAST and DWM-FAST results show clear deviations from each other suggesting that introducing the correct wake physics into such analysis is crucial, in fact for both up-wind and down-wind wind turbines. In an SHM context, this points out that, in the absence of direct loads measurements on a up-wind and wake-affected wind turbines, quantifying the mean wind speed and turbulence intensity for the purpose of surrogating/predicting the structural fatigue loads is necessary but not sufficient, additional signals indicating the wake signature are required. Similar results are generally observed for a separation distance of $D = 8$ rotor diameters between the up-wind and down-wind wind turbines.

In Fig. 5(c)-7(c) the ambient free-stream mean wind speed is $U = 20\ m/s$ which means that the up-wind wind turbine is operating in full load regime (producing at rated power) corresponding to a much lower thrust coefficient and induction. The remarks in the previous paragraph can be repeated here with regard to the fact that DEL of down-wind (wake-affected) wind turbine is lower compared to DEL of the up-wind wind turbine. However, at higher turbulence intensities ($Ti = 20\ \%$) both the standalone FAST and DWM-FAST simulations start to converge suggesting that the small scale mixing in the wake become so pronounced that the large scale effects of wake meandering are far less important. Indeed this is due to less efficient transport of the wake meandering resulting from lower thrust coefficient and induction.

In summary, at low mean wind speeds and low turbulence intensity OR at high mean wind speeds and high turbulence intensity an exact knowledge of the wake structure and wake signature are not necessary and only rotor averaged envi-

ronmental variables could be used to surrogate/predict the structural loads in the absence of direct loads measurements on a wake-affected wind turbine. Otherwise, additional signals indicating the wake signature are crucial and may lead to significant errors in DEL estimates and consequently life-cycle assessments (remaining useful lifetime of a component).

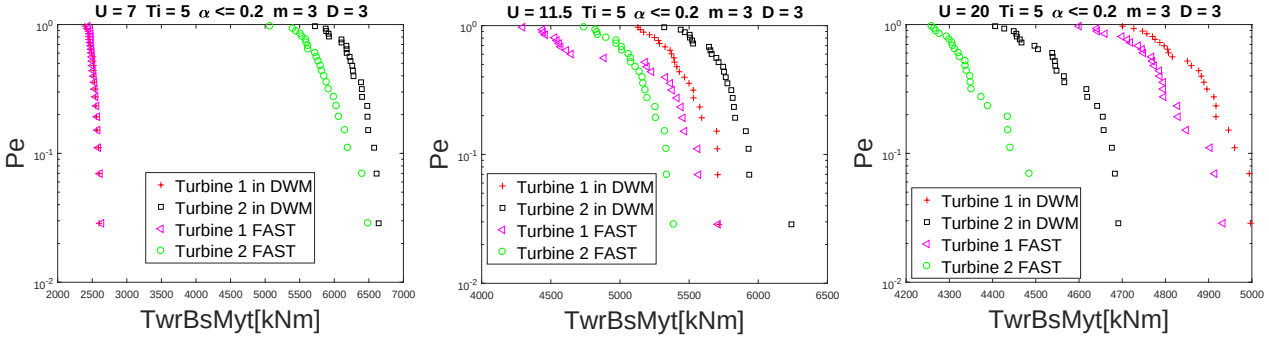


(a) (b) (c)

Figure 5: Probability of exceedance of the short-term DEL of the tower bottom fore-aft bending moment when $Ti = 5$ %, $m = 3$, and 3D separation (a) $U = 7\ m/s$. (b) $U = 11.5\ m/s$. (c) $TU = 20\ m/s$.

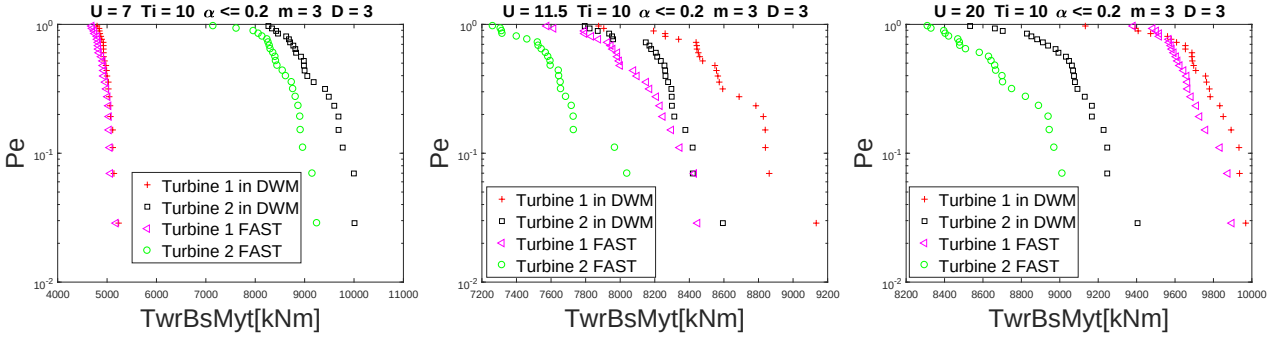


(a) (b) (c)

Figure 6: Probability of exceedance of the short-term DEL of the tower bottom fore-aft bending moment when $Ti = 10$ %, $m = 3$, and 3D separation (a) $U = 7\ m/s$. (b) $U = 11.5\ m/s$. (c) $TU = 20\ m/s$.

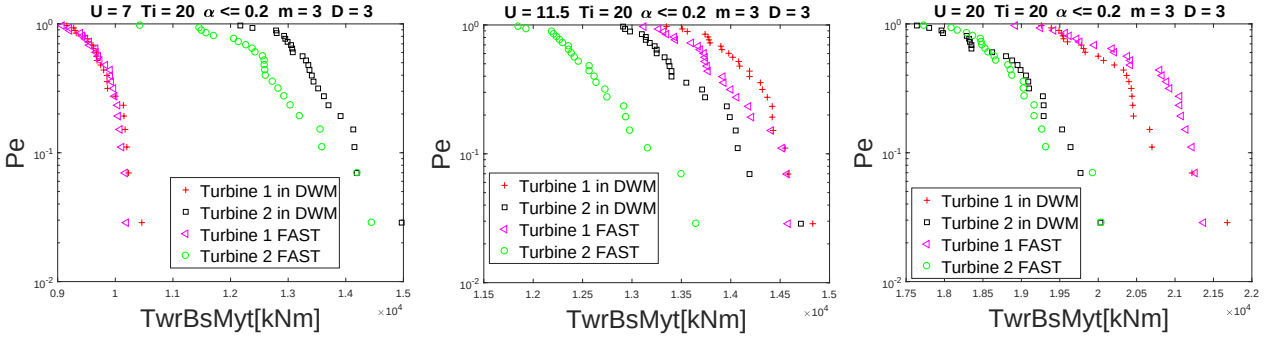


(a) (b) (c)

Figure 7: Probability of exceedance of the short-term DEL of the tower bottom fore-aft bending moment when $Ti = 20$ %, $m = 3$, and 3D separation (a) $U = 7\ m/s$. (b) $U = 11.5\ m/s$. (c) $TU = 20\ m/s$.

### *4.1.2 Blade*

At $U = 7\ m/s$ the high thrust coefficient and induction induce a significant wake deficit (lower wind speed in the wake) and an increase in turbulence. In the wake, the mean wind speed drops while the turbulence intensity increases; The increased turbulence experienced by a wake-affected wind turbine consists of two main contributions. The first contribution is an increased level of small-scale turbulence due the breakdown of tip vortices and turbulence generated by the shear layer in the edges of the wake. The other contribution comes from the meandering of the wake deficit relative to the position of the wake-affected rotor (Keck, 2013). This increase in turbulence explains why the short-term DEL of the down-wind (wake-affected) wind turbine is higher compared to DEL of the up-wind wind turbine as shown in Fig. 8(a).

However, this comparison does not hold any longer for all other mean wind speeds and turbulence intensities analysed in this paper, where the drop in the mean wind speed of the wind field in the wake-affected wind turbine becomes the main driver of the short-term DEL of the blades.

Furthermore, and unlike the tower, for ambient turbulence intensities (e.g. $Ti \geq 10$ %) and regardless of the mean wind speed, we observe that both the standalone FAST and DWM-FAST simulations results display the same trend for the short-term DEL of the down-wind (wake-affected) wind turbine. This suggests that introducing the correct wake physics into such analysis is NOT crucial. This is however not the case for lower mean wind speed and turbulence intensity as depicted in Fig. 8(a) and Fig. 8(b).

In an SHM context, this points out that, in the absence of direct loads measurements on a wake-affected wind turbine, quantifying the mean wind speed and turbulence intensity for the purpose of surrogating/predicting the structural fatigue loads is sufficient and additional signals indicating the wake signature are not required except for low turbulence and low mean wind speed operating conditions. Similar results are generally observed for a separation distance of $D = 8$ rotor diameters between the up-wind and down-wind wind turbines.

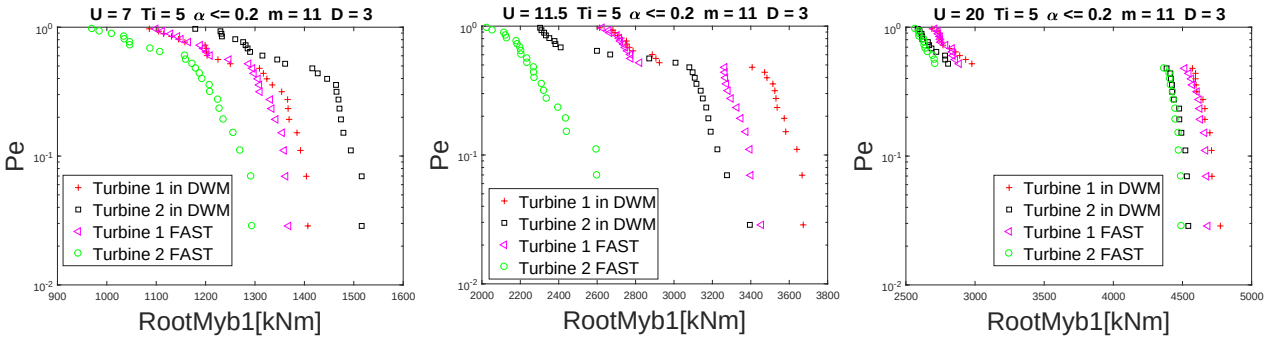


(a) (b) (c)

Figure 8: Probability of exceedance of the short-term DEL of the blade root flapwise bending moment when $Ti = 5$ %, $m = 3$, and 3D separation (a) $U = 7\ m/s$. (b) $U = 11.5\ m/s$. (c) $TU = 20\ m/s$.

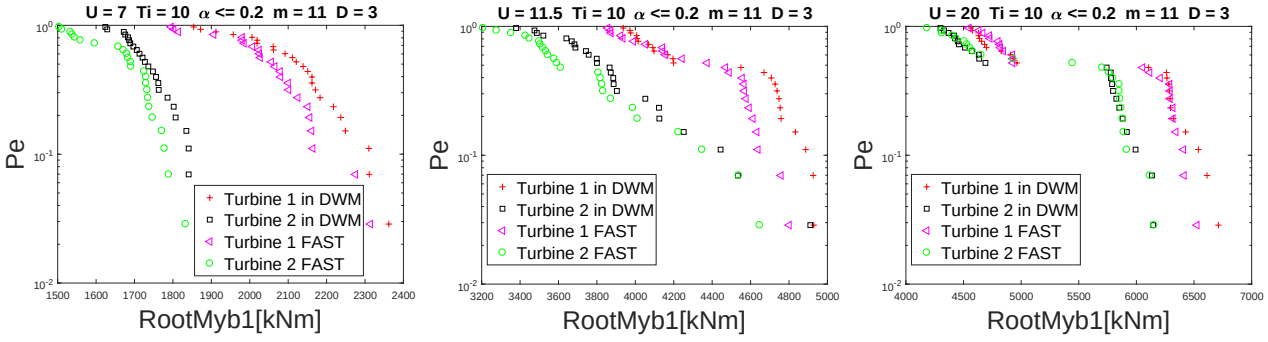


(a) (b) (c)

Figure 9: Probability of exceedance of the short-term DEL of the blade root flapwise bending moment when $Ti = 10$ %, $m = 3$, and 3D separation (a) $U = 7\ m/s$. (b) $U = 11.5\ m/s$. (c) $TU = 20\ m/s$.

### *4.1.3 Sensitivity analysis*

In an attempt to generalize the above observations and to better understand how the various environmental variables affect the DEL of the tower and blade, we will perform a sensitivity analysis. Sensitivity analysis is the study of how the uncertainty in the output of a model (mathematical, numerical or otherwise) can be apportioned to different sources of uncertainty in its inputs. In particular we will use the Standard Regression Coefficients (SRC) and the Standard Rank Regression Coefficients (SRRC) sensitivity analysis methods. SRC and SRRC are part of the linearized methods and are based on the post-processing of available samples of the model by performing a linear regression of the output on the input vector. They are rather simple as they do not require special sampling strategies. The sensitivity analysis is performed in the UQLab software (Marelli and Sudret, 2014, Marelli et al., 2015). For an up-to-date review and classification of sensitivity analysis techniques, please see Ioos and Lemaître (2015).

The sensitivity analysis results in Fig. 11 indicate that the short-term DEL of the blade root flapwise bending moment of the up-wind wind turbine (turbine 1) is marginally more sensitive to the mean wind speed compared to the turbulence intensity and the wind shear exponent; the difference is not significant between the three variables. However we observe that the mean wind speed becomes significantly more dominant in wake-affected wind Turbine (wind turbine 2) compared

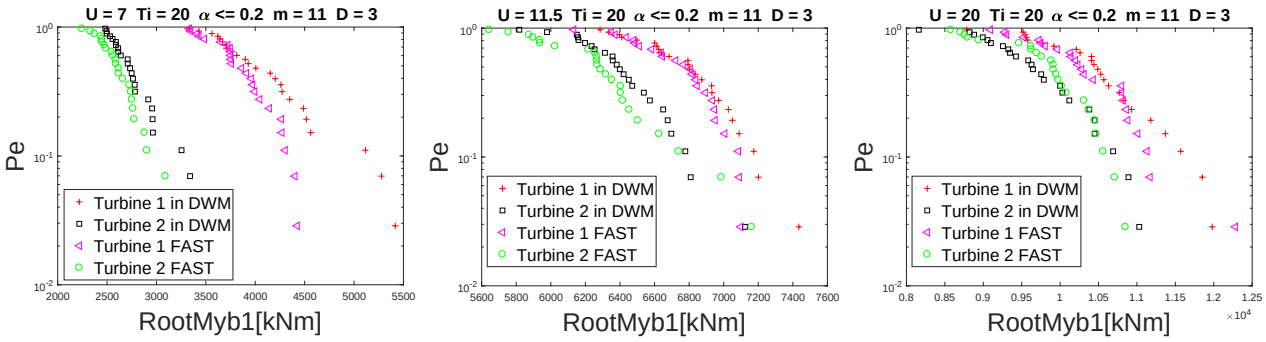


(a) (b) (c)

Figure 10: Probability of exceedance of the short-term DEL of the blade root flapwise bending moment when $Ti = 20$ %, $m = 3$, and 3D separation (a) $U = 7\ m/s$. (b) $U = 11.5\ m/s$. (c) $TU = 20\ m/s$.

to wind turbine 1.

Contrary to the wind turbine blade, variations in the short-term DEL of the tower bottom fore-aft bending moment, is dominated by the input turbulence intensity for both Turbines 1 and 2, and shear is deemed unimportant.

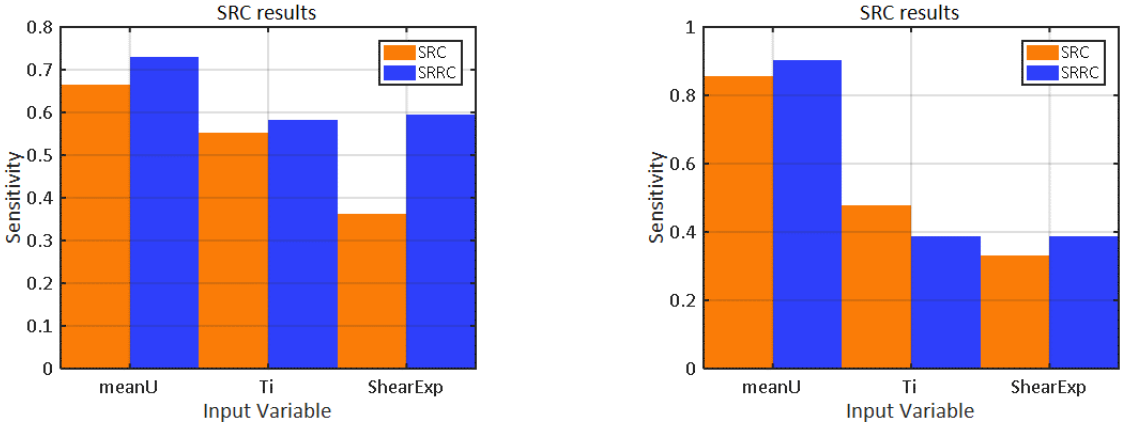


(a) (b)

Figure 11: SRC and SRRC sensitivity analysis results of the blade root flapwise bending moment DEL. (a) up-wind wind turbine 1 (b) down-wind (wake-affected) wind turbine 2.

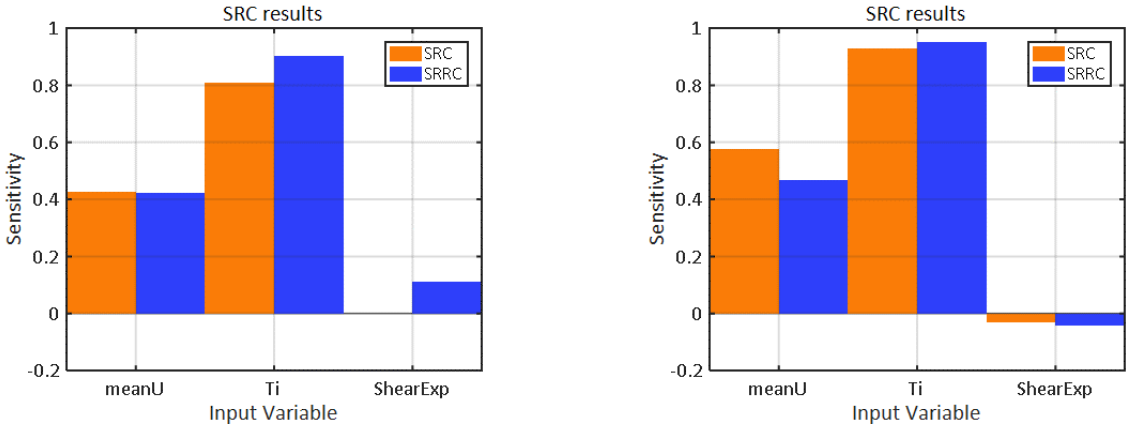


(a) (b)

Figure 12: SRC and SRRC sensitivity analysis results of the tower bottom fore-aft bending moment DEL. (a) up-wind wind turbine 1 (b) down-wind (wake-affected) wind turbine 2.

## 4.2 Analysis based on Gaussian Process time-series modeling

### *4.2.1 Construction of the baseline model*

In this section we attempt at determining if the dynamic characteristics of the loads of the wind turbine in the up-wind and waked configurations are different. To that end, a GP-LPV-VAR model is constructed as a surrogate of the loads in the tower base (fore-aft and lateral) and the blade root (flapwise and edgewise) as a function of the instantaneous rotor azimuth ($\beta[t]$), the 10 minute mean wind speed $U$, and the 10 minute mean turbulence intensity $Ti$. The model is built from a new set of simulations computed by FAST on the same wind turbine on a dense grid of mean wind speeds and turbulence intensities with the following values: $U = \{3,4,5,\ldots,25\}$, $Ti = \{4,8,12,\ldots,20\}$. For each value of the grid, six different seeds are used to create a simulation, using the same settings as those used to create the previous set of simulations. A total of 690 simulations are thus obtained. The obtained loads are then centered (mean subtracted) and resampled at 10 Hz. The instantaneous rotor azimuth is also resampled at 10 Hz.

The structure of the global GP-LPV-VAR model is accomplished in two stages: (*i*) identification of a simpler LPV-VAR structure; (*ii*) identification of the whole GP-LPV-VAR structure.

For the first stage, the cross-validation prediction error and Bayesian Information Criterion curves, and the frequency stabilization plot are utilized to determine the structure of simpler LPV-VAR models from data of a single simulation. A sinusoidal LPV-VAR functional basis is selected, so that $f_1(\beta[t]) = 1$, $f_{2k}(\beta[t]) = \cos\beta[t]$ and $f_{2k+1}(\beta[t]) = \sin\beta[t]$, for $k = 1,\ldots,(p_f-1)/2$, where $\beta[t]$ is the instantaneous rotor azimuth in radians. Parameter estimates are obtained by means of the prediction error method. This process leads to a LPV-VAR model structure with $n_a = 28$ and $p_f = 7$. Reduced representation dimensionality is attempted by means of the PCR approach, where the SVD results from the analysis of the sample regression matrix $\boldsymbol{\Phi}$ as in Equation (9). While the original LPV-VAR model is characterized by a dimensionality of $d = n_a \cdot p_f \cdot M^2 = 28 \cdot 7 \cdot 4^2 = 3\,136$ parameters, PCR leads to a representation with reduced dimensionality equal to $\tilde{d} = 400$ parameters.

Subsequently, the complete GP-LPV-VAR model is constructed. The hyperparameters are estimated by means of a suboptimal sample-based approach, where the coefficient matrix $\boldsymbol{M}$, the innovations covariance matrix $\boldsymbol{\Sigma}_w$ and the parameter covariance matrix $\boldsymbol{\Sigma}_\theta$ are estimated from sample averages of the parameter vectors $\hat{\boldsymbol{\vartheta}}_r$ and prediction errors $\boldsymbol{\varepsilon}_r[t]$ of simpler LPV-VAR models of each one of the $N_s = 690$ simulations. More specifically, each one of the hyperparameters is estimated as follows:

$$\hat{\boldsymbol{M}} = \hat{\boldsymbol{\Theta}} \cdot \boldsymbol{G}^T \cdot \left(\boldsymbol{G} \cdot \boldsymbol{G}^T\right)^{-1}, \qquad \hat{\boldsymbol{\Sigma}}_\theta = \frac{1}{N_s} \cdot \left(\hat{\boldsymbol{\Theta}} - \hat{\boldsymbol{M}} \cdot \boldsymbol{G}\right) \cdot \left(\hat{\boldsymbol{\Theta}} - \hat{\boldsymbol{M}} \cdot \boldsymbol{G}\right)^T, \qquad \hat{\boldsymbol{\Sigma}}_w = \frac{1}{N \cdot N_s} \sum_{r=1}^{N_s} \sum_{t=1}^{N} \boldsymbol{\varepsilon}_r[t] \cdot \boldsymbol{\varepsilon}_r^T[t] \tag{13}$$

where $\boldsymbol{\varepsilon}_r[t] = \boldsymbol{y}_r[t] - \boldsymbol{\varphi}_r^T[t] \cdot \hat{\boldsymbol{\vartheta}}_r$ is the LPV-VAR model based prediction error, $\hat{\boldsymbol{\Theta}} = \begin{bmatrix}\hat{\boldsymbol{\vartheta}}_1 & \hat{\boldsymbol{\vartheta}}_2 & \cdots & \hat{\boldsymbol{\vartheta}}_{N_s}\end{bmatrix}$ is a matrix with the estimates of the parameter vectors of the sample $\hat{\boldsymbol{\vartheta}}_r$, $r = 1,\ldots,N_s$, and $\boldsymbol{G} = \begin{bmatrix}\boldsymbol{g}(\boldsymbol{\xi}_1) & \boldsymbol{g}(\boldsymbol{\xi}_2) & \cdots & \boldsymbol{g}(\boldsymbol{\xi}_{N_s})\end{bmatrix}$ is a matrix with the GP functional basis evaluated on the EOP vectors $\boldsymbol{\xi}_r$ corresponding to each simulation. The GP functional basis depends on the two EOPs of interest, namely the mean wind speed and the turbulence intensity, so that $\boldsymbol{\xi}_r := \begin{bmatrix}U_r & Ti_r\end{bmatrix}^T$. The basis is constructed by the Kronecker product of univariate cubic B-spline basis on each one of the EOPs. By trial and error, the order of the B-spline basis for the mean wind speed is selected as $p_1 = 10$, while that for the turbulence intensity is $p_2 = 5$, thus leading to a total number of $p = p_1 \cdot p_2 = 50$ basis.

In Fig. 13 are displayed the interpolated parameter surfaces corresponding to the expected values of the parameters $\vartheta_1$, $\vartheta_2$, $\log\sigma_1^2$ and $\log\sigma_2^2$ obtained with the GP-LPV-VAR model as a function of the mean wind speed and turbulence intensity. In addition, the estimates of the LPV-VAR model parameters on individual realizations are also displayed. The dependency of the parameters on the selected EOPs is clear. Likewise, it can be observed that the parameter surfaces predicted by the global GP-LPV-VAR model comply with the variations observed in the parameter values of LPV-VAR models on individual realizations. In particular, the parameters related to the innovations variance demonstrate a clear increment as the wind speed and turbulence intensity increase. This indicates that not only the wind speed is an important driver of the load amplitude, but also the turbulence intensity has a substantial effect in the loads. On the other hand, the effect of turbulence intensity is less evident in the AR parameters, which suggests that the dynamics of the wind turbine loads are less influenced by turbulence.

Further analysis of the global dynamics of the wind turbine loads can be achieved based on the obtained GP-LPV-VAR model. For instance, the average natural frequencies and damping ratios may be obtained from the constant terms of the parameter matrices of the LPV-VAR model. In fact, the VAR model defined by the equation:

$$\boldsymbol{y}[t] = \sum_{i=1}^{n_a} \boldsymbol{A}_{i,1} \cdot \boldsymbol{y}[t-i] + \boldsymbol{w}[t] \tag{14}$$

corresponds to the *Best Linear Time Invariant* (Best LTI) approximation of the time-dependent system determined by the LPV-VAR model. Therefore, modal analysis on the parameter matrices of the Best LTI approximation yields the mean components of the natural frequencies and damping ratios.

Fig. 14 displays the modal analysis results based on the Best LTI approximation of the GP-LPV-VAR model for increasing mean wind speed and turbulence intensity. Fig. 14a displays the natural frequencies and damping ratios for

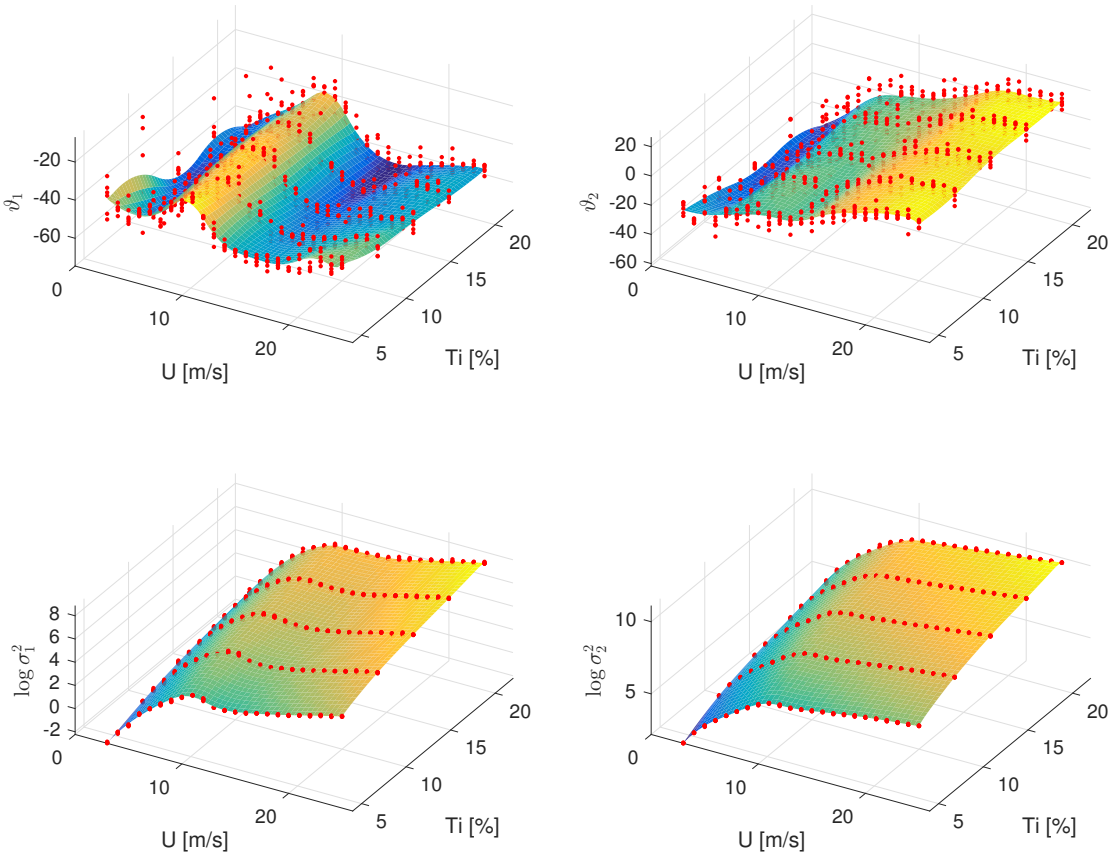


Figure 13: Surfaces displaying the expected value of the parameters $\vartheta_1$, $\vartheta_2$, $\log \sigma_1^2$ and $\log \sigma_2^2$ of the GP-LPV-VAR model as a function of the mean wind speed and turbulence intensity. Overlaid red dots indicate the values of the LPV-VAR model parameter estimates of individual simulations.

increasing wind speed and fixed turbulence intensity at $Ti = 10$ %. On the other hand, Fig. 14b displays the same quantities as a function of turbulence intensity for fixed wind speed at 10 m/s. It can be observed that although the natural frequencies remain more or less constant, the damping ratios show important variations, in some cases going close to zero for certain wind speeds or turbulence intensities. In the present context, this means that the wind turbine will experience higher loads for specific configurations of wind speeds and turbulence intensities. More precisely, an important conclusion from Fig. 14b is that a wind turbine operating under higher turbulence intensities is prone to suffer higher amplitude loads related to the 1st tower fore-aft and side to side modes.

### *4.2.2 Analysis of the dynamics in the up-wind and waked wind turbines*

The obtained GP-LPV-VAR surrogate for the wind turbine loads is now used to compare the loads of the up-wind and waked wind turbines, and thus determine if there are important variations in the structural dynamics in the two configurations. To start with, Fig. 15 displays parameters $\vartheta_1$, $\vartheta_2$, $\log \sigma_1^2$ and $\log \sigma_2^2$ of the LPV-VAR model calculated for the up-wind and waked wind turbines for turbulence intensity $Ti = 10$ %. In addition, the corresponding GP-LPV-VAR model based mean and confidence intervals are also displayed. It can be observed that the LPV-VAR parameters of the wind turbines at both configurations adhere to the regions predicted by the GP-LPV-VAR model, except for lower wind speeds, where the parameters of the waked wind turbine tend to drift off from the expected value. Such difference is more evident in the innovations variance coefficients, which indicates that the model cannot predict effectively the load amplitudes at low wind speeds.

A more comprehensive analysis of these variations is accomplished by means of the Mahalanobis distances on the parameter and prediction errors shown in Eq. (6). In Fig. 16 are displayed the parameter and prediction error Mahalanobis distances evaluated on the whole set of simulations from the up-wind and waked wind turbines. Regarding to the parameter-based distances shown in Fig. 16a, it is observed that in overall the distances are larger for lower wind speeds and higher turbulence intensities. The largest differences are observed on the waked wind turbine at a distance of 3 diameters (3D). Significant deviations are also observed in the waked wind turbine at 8 diameters. These outcomes indicate that the dynamics of the waked wind turbines are slightly different from those of the wind turbine receiving clean wind, particularly at low wind speeds.

On the other hand, the prediction error distances displayed in Fig. 16b demonstrate that in general, the model can describe the dynamics of the loads in both up-wind and waked wind turbines approximately with the same precision.

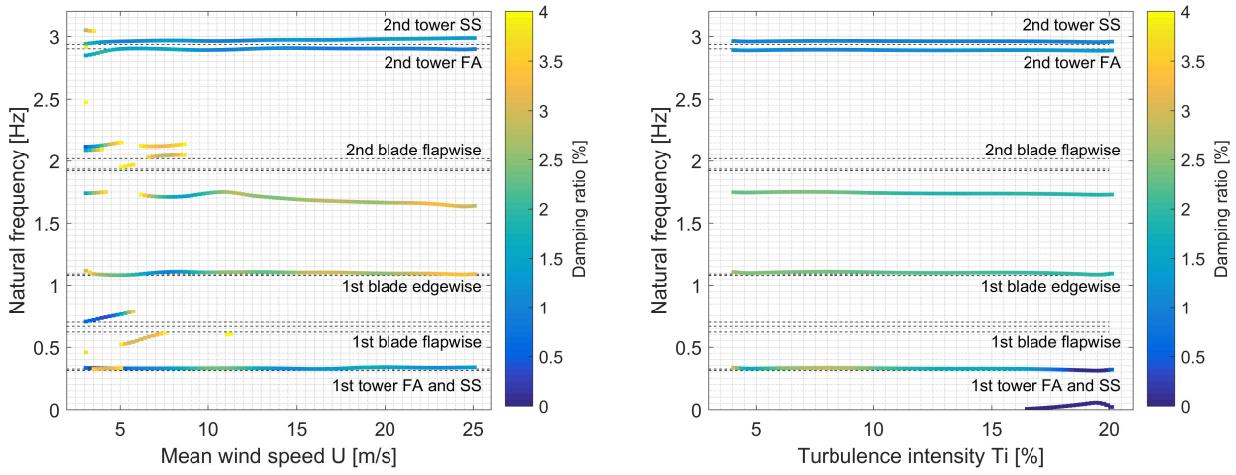


(a) (b)

Figure 14: Modal analysis of the wind turbine loads based on the Best LTI approximation of the LPV-VAR model: (a) natural frequencies and damping ratios as a function of mean wind speed for fixed $Ti = 10$ %, and (b) natural frequencies and damping ratios as a function of turbulence intensity with fixed $U = 10$ m/s. Only the modes with damping ratio lower than 4% are displayed. Horizontal dashed lines indicate the natural frequencies of structural modes estimated by FAST.

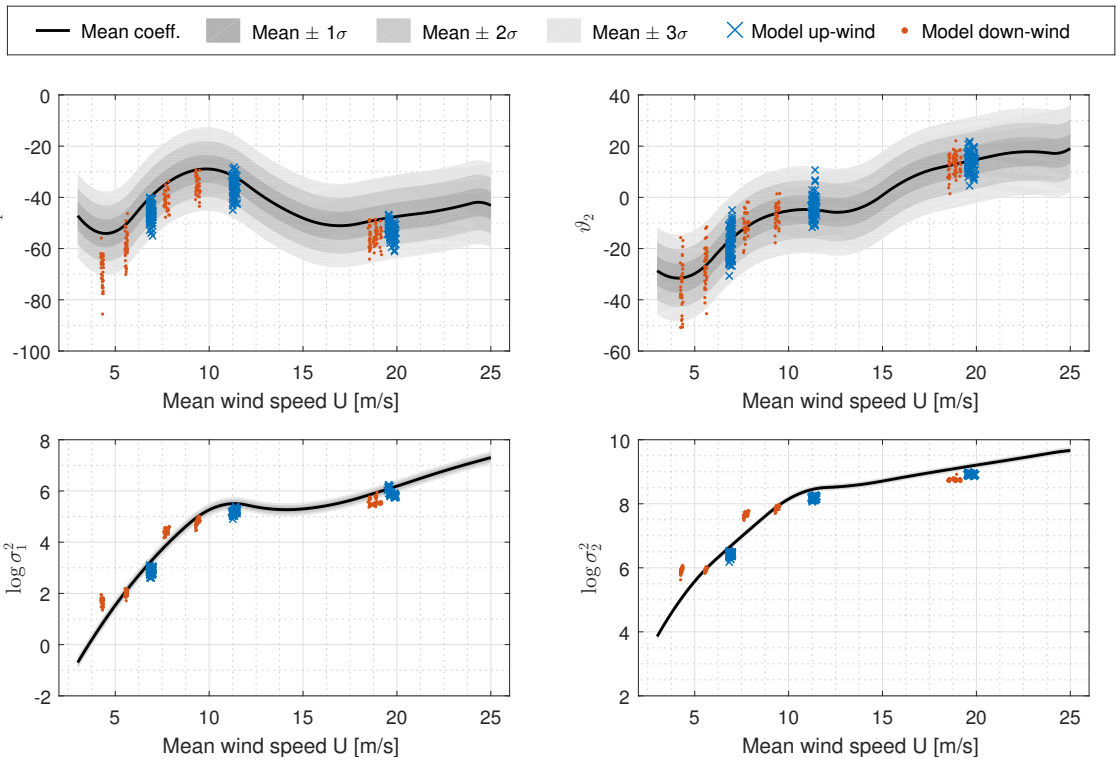


Figure 15: Mean and standard deviations of the parameters $\vartheta_1$, $\vartheta_2$, $\log\sigma_1^2$ and $\log\sigma_2^2$ predicted by the GP-LPV-VAR model, and corresponding LPV-VAR parameter estimates obtained from the simulation data of up-wind and waked wind turbines for a turbulence intensity of 10%.

However, some outliers are observed, related with turbulence intensities higher than 20%. Unfortunately, this difference stems from a deficiency during the training of the GP-LPV-VAR model, since the training set of simulations considers turbulence intensities only up to 20 %. Future improvements shall focus on creating simulations from an extended grid of EOPs, in order to create a broader representation of the load dynamics.

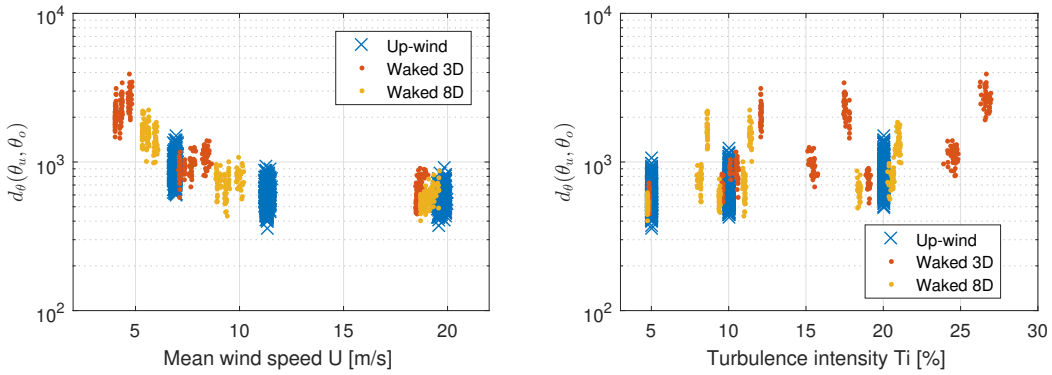


(a)

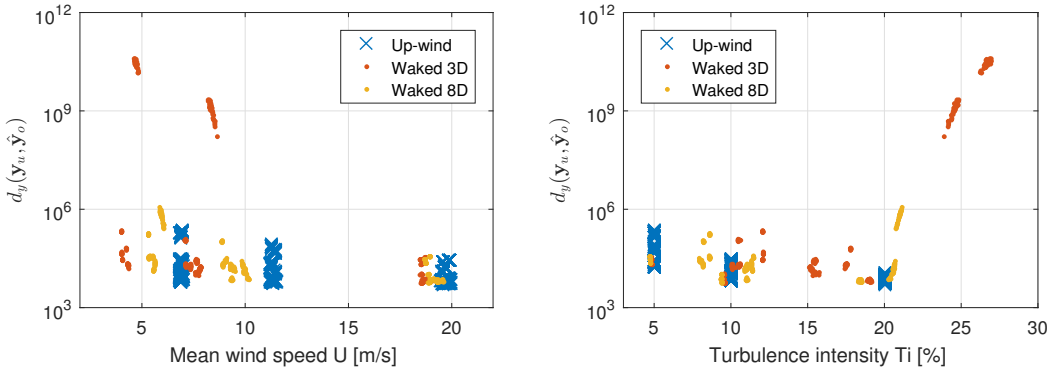


(b)

Figure 16: Distance measures obtained between the predictions of the baseline GP-LPV-VAR model and the values extracted from the up-wind and waked wind turbines: (a) Parameter-based Mahalanobis distances vs. mean wind speed (left) and turbulence intensity (right); (b) Prediction error based Mahalanobis distances vs. mean wind speed (left) and turbulence intensity (right).

## CONCLUSIONS AND OUTLOOK

The focus in this study, in the context of structural health monitoring and life-cycle assessment, is to define what features to look for (what to measure) and how accurately to measure these features, when direct structural and loads measurements of wake-affected wind turbines are not available.

To this end, we analyzed the differences in the dynamic response of an up-wind and a wake-affected wind turbines via surrogate GP time-series models, and short term damage equivalent fatigue loads (DEL). A full-factorial design of experiments was formulated based on variations in the mean wind speed $U$, turbulence intensity $Ti$, shear exponent $\alpha$, spacing between the up-wind and down-wind wind turbines, and the material properties of structural components, namely the Wöhler exponent. The aeroelastic response of the up-wind and wake-affected wind turbines were carried out for each of the input variables combinations via the DWM model coupled into FAST aeroelastic simulator. The output of interest were the flapwise bending moment at the blade root ($M_b$) and tower bottom fore-aft bending moment ($M_t$). To better understand the effect of wake physics on wind turbine fatigue loads, we supplement the DWM-FAST simulations with FAST aeroelastic simulations of a standalone wind turbine with input turbulent inflow characteristics corresponding to rotor averaged inflow conditions derived by DWM on both up-wind and down-wind wind turbines.

For the blade, the analysis of the short term damage equivalent fatigue loads indicate that in the absence of direct structural loads measurements on a wake-affected wind turbine, quantifying the rotor averaged input environmental conditions for the purpose of surrogating/predicting the structural fatigue loads is sufficient and additional signals indicating the wake signature (correct wake physics) are not required except for very low turbulence AND mean wind speeds below rated operating conditions ($Ti = 5\%$ & $U \leq U_{rated}$).

For the tower, at low mean wind speeds and low turbulence intensity ($U = 7\ m/s$ & $Ti = 5\%$) or at high mean wind speeds and high turbulence intensity ($U = 20\ m/s$ & $Ti = 20\%$) an exact knowledge of the wake structure and wake signature is not necessary and only rotor averaged environmental variables could be used to surrogate/predict the structural loads in the absence of direct loads measurements on a wake-affected wind turbine. Otherwise, additional signals indicating the wake signature are crucial and may lead to significant errors in DEL estimates and consequently life-cycle assessments (remaining useful lifetime of a component).

The sensitivity analysis results indicate that the short-term DEL of the blade root flapwise bending moment of the up-wind wind turbine is marginally more sensitive to the mean wind speed compared to the turbulence intensity and the

wind shear exponent. However we observe that the mean wind speed becomes significantly more dominant in the wake-affected wind turbine. Contrary to the wind turbine blade, variations in the short-term DEL of the tower base fore-aft bending moment, is dominated by the input turbulence intensity for both up-wind and down-wind wake-affected wind turbines, and shear is deemed unimportant. These results reflect how components with large Wöhler values (blades-composites) are sensitive to the few large load cycles, whereas components with small Wöhler values (tower-steel) are sensitive to many small cycles.

From a surrogate modeling perspective, the principal conclusion is that the loads in both up-wind and waked wind turbines can be accurately represented by a global model up to a certain reasonable limit. This is an important result, since potentially a single wind turbine could be monitored, while approximate load statistics on other wind turbines could be extrapolated from a single surrogate model. In the present implementation via GP-LPV-VAR modeling, main advantages stem from the implicit assessment of uncertainty on the model parameter and variances and compact representation of very complex dynamics. However, it is still necessary to further improve the model estimation procedures for large data sets as those utilized in the present context. The sub-optimal sample-based estimation procedure appraised in this work yields proper results, but more refined estimates could enhance the differences between the dynamic features of up-wind and waked wind turbines.

There are several essential extensions to this research. The first one is a more refined and comprehensive design of experiments to dig deeper into the effects of the environmental conditions on the short-term damage equivalent fatigue loads. The second is to investigate how higher fidelity aeroelastic simulators may affect the analysis of the dynamic response and consequently the calculations of the short-term damage equivalent loads, not only on blade root and tower bottom but other components as well such as tower top tilt and yaw as well as blade out-board flap and edgewise.

## ACKNOWLEDGEMENTS

The authors acknowledge the support of the European Research Council via the ERC Starting Grant WINDMIL (ERC-2015-StG #679843) on the topic of Smart Monitoring, Inspection and Life-Cycle Assessment of Wind Turbines. In addition, Dr. Avendaño-Valencia would like to further acknowledge the support of the ETH Zurich Postdoctoral Fellowship FEL-45 14-2 “A data driven computational framework for damage identification and life-cycle management of wind turbine facilities”.

## REFERENCES

Avendaño-Valencia, L.D., and Fassois, S.D., 2014, “Stationary and non-stationary random vibration modelling and analysis for an operating wind turbine”, Mechanical Systems and Signal Processing, 47(1-2), 263-285.

Avendaño-Valencia, L.D., Chatzi, E. N., Fassois, S.D., 2017, “Sensitivity driven robust vibration-based damage diagnosis under uncertainty through hierarchical Bayes time-series representations”, Procedia Engineering, 199, 1852-1857.

Avendaño-Valencia, L.D., and Fassois, S.D., 2017, “In-operation wind turbine modal analysis via LPV-VAR modeling”, In: D. Di Maio, P. Castellini (eds.), Rotating Machinery, Hybrid Test Methods, Vibro-Acoustics & Laser Vibrometry, Volume 8. Conference Proceedings of the Society for Experimental Mechanics Series. Springer.

Avendaño-Valencia, L.D., and Chatzi, E. N., 2017, “Sensitivity driven robust vibration-based damage diagnosis under uncertainty through hierarchical Bayes time-series representations”, Procedia Engineering, 199, 1852-1857.

Avendaño-Valencia, L.D., Chatzi, E. N., and Brownjohn, J., 2017, “Metamodeling of the dynamic response of structures under uncertainty via Gaussian Process time-series models”, submitted to Frontiers in Built Environment.

Frandsen, S.T. and Thoegersen, M.L., 2000, “Integrated Fatigue Loading for Wind Turbines in Wind Farms by Combining Ambient Turbulence and Wakes”, Wind Engineering, Volume 23, No. 6.

Frandsen, S.T., 2007, “Turbulence and turbulence-generated structural loading in wind turbine clusters”, Risø-R-1188(EN), Risø National Laboratory, Roskilde, Denmark.

Häckell, M.W., and Rolfes, R., 2013, “Monitoring a 5MW offshore wind energy converter – Condition parameters and triangulation based extraction of modal parameters”, Mechanical Systems and Signal Processing, 40, 322-343.

Hao, Y., Lackner, M. A., Keck, R.E., Lee, S., 2014, Churchfield, M. J., and Moriarty, P., “Implementing the Dynamic Wake Meandering Model in the NWTC Design Codes”, Proceedings of 32nd ASME Wind Energy Symposium, National Harbor, Maryland, AIAA, Wahington, DC, AIAA Paper 2014-1089.

Iooss, B. and Lemaître, P., 2015 “A review on global sensitivity analysis methods”, In C. Meloni and G. Dellino (Eds.), Uncertainty management in Simulation-Optimization of Complex Systems: Algorithms and Applications. Springer.

Jonkman, J., Buhl, M., 2005, “FAST user’s guide”, Tech. Rep. NREL/EL-500-38230, National Renewable Energy Laboratory.

Jonkman, J, Butterfield, S., Musial, W., and Scott, G., 2009, “Definition of a 5-MW Reference Wind Turbine for Offshore System Development”, NREL/TP-500-38060, Golden, CO: National Renewable Energy Laboratory.

Kaimal, J.,Wyngaard, J. and Coté O., 1972, “Spectral characteristics of surface-layer turbulence”, Quart J R Met Soc, 98:563–589.

Keck, Rolf-Erik, 2013, “A consistent turbulence formulation for the dynamic wake meandering model in the atmospheric boundary layer”, DTU Wind Energy, 219 p. (DTU Wind Energy PhD; No. 0012(EN)).

Larsen, T.J., Madsen, H. A., Larsen, G.C. and Hansen, K.S., 2013, “Validation of the Dynamic Wake Meander Model for Loads and Power Production in the Egmond aan Zee Wind Farm”, Wind Energy, Volume 16, Issue 4, pp. 605–624.

Larsen, G. C., Madsen Aagaard, H., BingÃ¶l, F., Mann, J., Ott, S., SÃ¸rensen, J. N., and Mikkelsen, R., 2007, “Dynamic wake meandering modeling”, Risø National Laboratory. (Denmark. Forskningscenter Risoe. Risoe-R; No. 1607(EN)).

Lee, S., Churchfield, M., Moriarty, P., Jonkman, J., and Michalakes, J., 2012, “Atmospheric and wake turbulence impacts on wind turbine fatigue loading”, NREL/CP-5000-53567, DOI: 10.2514/6.2012-540.

Madsen, H.A., Thomsen, K. and Larsen, G.C., 2003, “A New method for Prediction of Detailed Wake Loads”, Proceedings of IEA Joint Action of Wind Turbines 16th Symposium held in Boulder, USA, NREL, edited by Sven-Erik Thor. pp. 171-188.

Marelli, S. and Sudret, B., 2014, “UQLab: A framework for uncertainty quantification in Matlab”, Vulnerability, Uncertainty, and Risk (Proc. 2nd Int. Conf. on Vulnerability, Risk Analysis and Management (ICVRAM2014), Liverpool, United Kingdom), pp2554-2563, ch. 257.

Marelli, S., Lamas, C. and Sudret, B., 2015, “UQLab user manual – Sensitivity analysis, Report UQLab-V0.9-106”, Chair of Risk, Safety & Uncertainty Quantification, ETH Zurich.

Ozbek, M., Meng, F., and Rixen, D.J.; 2013, “Challenges in testing and monitoring the in-operation vibration characteristics of wind turbines”, Mechanical Systems and Signal Processing, 41, 649-666.

Schmidt, B., King, J., Larsen, G.C., and Larsen, T.J., 2011, “Load validation and comparison versus certification approaches of the Risø Dynamic Wake Meandering (DWM) model implementation in GH Bladed”, EWEA annual event, Brussels, Belgium.

Shirzadeh, R., Devriendt, C., Bidakhvidi, M.A., and Guillaume, P., 2013, “Experimental and computational damping estimation of an offshore wind turbine on a monopile foundation”, Journal of Wind Engineering and Industrial Aerodynamics 120, 93-106.

Thomsen, K., Madsen H.Aa and Larsen G.C., 2003, “A new method can predict detailed response for turbines in wind farms”, Fact sheet AED-RB-16 (EN), Risoe National Laboratory, Roskilde, Denmark

Vølund, P., 1992, “Loads on a horizontal axis wind turbine operating in wakes”, Journal of Wind Engineering and Industrial Aerodynamics 39(1), 317-328.

## RESPONSIBILITY NOTICE

The authors are the only responsible for the printed material included in this paper.